Stanford Exploration Project, Report 92, November 12, 1997, pages 31–52

Stanford Exploration Project, Report 92, November 12, 1997, pages 31–52

Revealing geological discontinuities by local plane wave suppression

Matthias Schwab, Curt Holden, and Jon Claerbout[1]

keywords: *deconvolution, two-dimensional, modeling, faults, amplitudes, Fourier transform, graphics, acquisition*

ABSTRACT

Interpreters of migrated seismic image volumes need to delineate reflector discontinuities, such as faults or buried channels. To enhance these discontinuities we applied local, data-adaptive Prediction Error (PE) Filters to the migrated image. We restricted the PE Filters to local combinations of 2-D filters, which remove local planar events and reveal rapidly varying local features. Unfortunately, while the scheme successfully enhanced geological discontinuities in one field data case, it failed in two others. In these two cases, the PE Filters erroneously predicted (and consequently removed) the geological discontinuities of interest. We were unable to tune the PE Filters to forgo a specific target bandwidth. Such a tuning may be possible if we use a sequence of two PE filtering steps of which the first filter prewhitens the image. In another case, the PE filter enhanced the image's acquisition footprint and thereby obliterated any geological details. Moreover, we do not yet know how to combine optimally the various PE Filter residuals to produce a meaningful subsurface map.

INTRODUCTION

Interpreters analyze migrated seismic data to map the subsurface geology. Unfortunately, the seismic data image, which is a back-propagated wave-field, does not represent all geological features equally well. The general wave-field character of the migrated image sometimes conceals important geological details, such as faults and river channels. Interpreters, however, seek faults and river channels since they indicate the location and properties of potential reservoirs.

Faults and river channels do not always cause easily discernible image patterns. Interpreters often delineate faults and river channels indirectly by identifying their effect on surrounding reflectors. The seismic wave-field often does not contain fault reflections, since the fault reflects seismic energy poorly or, if the fault dips steeply,

[1]**email:** matt@sep.stanford.edu, curt@sep.stanford.edu, jon@sep.stanford.edu

the reflection energy is not recorded or imaged. A fault, however, offsets the neighboring geological strata, which causes a discontinuity of the seismic reflectors. Similarly, river channels usually cut their neighboring geological strata in characteristically meandering patterns. Interpreters search for these reflector discontinuities when locating faults or river channels in a seismic image volume. A seismic image volume that enhances the subsurfaces discontinuities enables interpreters to map faults and river channels quickly and accurately.

What computational process, then, enhances discontinuities? In general, a roughening filter, such as a gradient or a second derivative, enhances discontinuities. Moreover, an ideal roughening filter for detecting faults and river channels should

- be robust with respect to noise in the migrated image
- have high resolution
- be inexpensive to apply
- be easy to adapt to various data sets and targets.

Discontinuities vary in size. Some faults are only a single sample wide while others span several pixels and appear as transition zones of rapid change. Ideally, a processor could tune the filter process to any target by setting a few well-understood parameters.

Claerbout(**?**) suggests using a pair of PE Filters to enhance discontinuities in a seismic image volume. Data-adaptive PE filter techniques promise high spatial image resolution. In general, the PE filter output tends to have a white spectrum, but the filter response can be indirectly tuned by the choice of the filter shape.

In this article, we extend Claerbout's earlier work: we apply three filters simultaneously and we exclusively focus on image processing for geological interpretation. We resurrected Claerbout's earlier work because Bahorich and Farmer(1995), Haskell(1995), and Nissen(1995) obtained impressive results from similar research. All the processes that attempt to enhance discontinuities are sensitive to noise. Marfurt(1995) discusses difficulties with coherent noise caused by the recording geometry of the seismic data (acquisition footprint).

FILTER TECHNIQUE

The Earth's geology changes with location. Most areas of oil exploration are dominated by sedimentary rocks, which despite their original flat deposition, are often faulted, folded, and partially eroded. At most locations, however, the seismic subsurface image of such sedimentary rocks can be locally approximated by a set of smooth, parallel, planar reflectors. The local approximation of dipping 2-D sedimentary beds in 3-D by small *plane reflector volumes* matches the familiar approximation of a 2-D curve by short straight line segments. Occasional discontinuities, such as faults or erosional surfaces, demarcate these smoothly-varying reflector volumes. To map these occasional discontinuities, we intend to estimate and remove the plane reflector contribution at each subsurface location. The estimation is bound to fail where discontinuities violate our assumption of a local, parallel, planar model. The subsequent removal yields a large residual. The scheme does not detect the discontinuity itself but the interrupting effect it has on its surrounding neighboring plane reflector volume. In other words, the proposed approach looks at three scales of the subsurface image. It breaks down the overall image (first scale), to small mostly homogeneous subcubes (second scale). The approach estimates and removes the plane reflector contribution in these subcubes and thereby exposes the discontinuities (third scale) that violate the model of a single plane reflector volume.

Monoplanes in local windows

To estimate and remove the local plane reflector component, we split the non-stationary seismic image into small local stationary cubes (see Figure 1). In each subcube, a filter step independently estimates and removes the plane reflector component. The filter output, those events the filter could not remove, are ultimately merged into an image volume of the same size as the original unfiltered image.

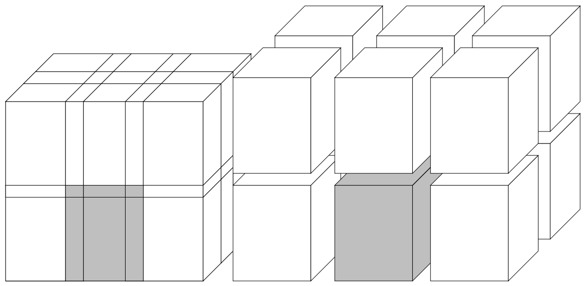

Figure 1: Left is the data input and output volume. Right is the data structure during analysis. matt2-rayab3D [NR]

The choice of the subcube's size depends on the non-stationarity of the processed image. A very large subcube would probably not fit the model of a single plane reflector (just as a large curve segment is probably not well approximated by a straight-line segment). In contrast, a very small subcube would probably not permit a reliable estimate of the local reflector component. Ideally the subcube size should depend on the local stationarity of an image. We, however, used existing routines for splitting and merging the image(Claerbout, 1994). These routines require the user to specify a single, general subcube size which is applied equally to the entire image. We typically chose subcubes of the size $(n1, n2, n3) = (15, 8, 8)$, where $n1$ refers to the number of samples in the depth or time dimension, and $n2, n3$ to the number of samples in the two horizontal dimensions. We overlapped the subcubes by 50%. We have not discovered any artifacts introduced into the processed figures by the software that splits and merges the data.

Rejection of a single plane reflector volume

A field of tilted parallel planes (such as the plane reflectors discussed above) can be mathematically represented as $f(x,y,z) = g(p_x x + p_y y + p_z z)$ where $g()$ is an arbitrary one-dimensional function. There are various filters that destroy such a field of parallel planes. A convenient low order filter that destroys such a field is the three-component operator $(p_y\partial_z - p_z\partial_y,\ -p_x\partial_z + p_z\partial_x,\ p_x\partial_y - p_y\partial_x)$. If and only if the input data is a field of tilted parallel planes, we can find parameters p_x, p_y, p_z so that all three output volumes vanish (see the Appendix). We can solve for the correct parameters p_x, p_y, p_z by minimizing the power of the filtered data.

Instead of finite-difference operators, we decided to use related PE filters. Finite-difference representations of differential operators are susceptible to accuracy problems known in finite-difference wave propagation as "frequency dispersion". PE filters are not as susceptible to dispersion as finite difference operators. Furthermore, PE filters can deal with aliased data(Claerbout, 1994).

A planar or 2-D PE filter

$$\begin{array}{cc} f & a \\ g & b \\ 1 & c \\ \cdot & d \\ \cdot & e \end{array} \tag{1}$$

corresponds to a finite-difference operator $p_z\partial_x - p_x\partial_z$. The vertical axis is z (depth or time), the horizontal axis is x (lateral location) and the "·"s are zeros. Imagine all the coefficients vanished but $d = -1$ and the given 1. Such a filter would annihilate the appropriately sloping plane wave. Slopes that are not exact integers are also approximately extinguishable because the adjustable filter coefficients can interpolate in time. Filters such as (1) affect the operation $p_z\partial_x - p_x\partial_z$, which is a component of the gradient in the local set of planes, and they include a temporal deconvolution aspect and a spatial coherency aspect.

To reject an image's existing plane reflector contribution of an unknown dip, we find the filter coefficients of filter (1) that when convolved with the image yield a minimal output (residual). This set of filter coefficients is the solution of a linear inverse problem, which we solve by a conjugate gradient algorithm.

The equivalent to a three component finite difference operator $(p_y\partial_z - p_z\partial_y,\ -p_x\partial_z + p_z\partial_x,\ p_x\partial_y - p_y\partial_x)$ is a combination of three planar PE filters. As Figure 2 indicates, each planar filter predicts the data in a plane vertical to any other plane. To find the three filters that reject a plane reflector volume of unknown dip, we independently solve an individual inverse problem for each filter.

Currently, we routinely apply the planar filters on all three dimensions of the image cube, resulting in three residual volumes for each subcube. All subcubes related to a single filter direction are merged back to the original image volume, resulting in a total of three residual volumes. We have not yet found an appropriate method of

Figure 2: An East-West, a North-South, and a time-slice 2-D PE filter all applied throughout the volume. To find each filter, minimize each output power independently. matt2-rayab3Doper [NR]

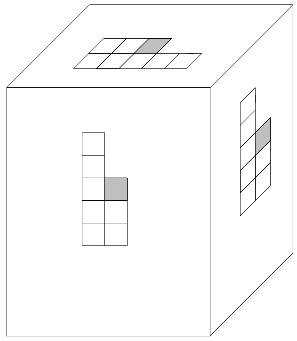

combining these three outputs to a single residual volume.

The shape of a 2-D PE filter is constrained by its objective: the filter's height can be changed, but its width has to remain two columns wide. Two columns can destroy a single plane, which corresponds to our model of a single plane reflector dip within a subcube. Any additional column could destroy an additional plane and consequently could remove more energy than the single plane reflector model justifies. The length of the 2-D PE filter has to be larger than the maximal stepout (dip) of the input data. We typically choose the filter length 7, yielding a filter with 10 unknown coefficients.

By forcing a 1-D, two-term filter to predict both backward and forward, we avoid perfect predictability on growing 1-D exponentials(Claerbout, 1976). To prevent predictions of exponentially growing planes, we require the 2-D PE filter to extinguish two copies of the data: the original copy and a second copy with both x and z reversed. Dips on the reversed copy are the same as on the original, but amplitude growth on one is decay on the other.

We will refer to the combined process of splitting the input image into subcubes, suppressing the local planar event in each subcube, and finally merging the subcubes to the residual image, as *Lomoplan*. Lomoplan has as many output cubes as the number of PE filters applied to each subcube (usually 3). Each final output cube is the size of the input volume.

SYNTHETIC EXAMPLES

The synthetic subsurface image in Figure 3 simulates a delta with a slump fault. The model has horizontal layers near the top, a Gaussian appearance (the delta sediments) in the middle, and dipping layers on the bottom. Horizontal unconformities divide the three regions.

The left image of Figure 3 shows a horizontal time-slice from the middle of the model. A careful observer will notice the parabolic fault line in the center of the plot (Figure 4 displays the slump fault's location more visibly and may help locating it in Figure 3). The image in the center shows a vertical slice that corresponds to a cut in the North-South direction of the original model. (In general, we use by North-South

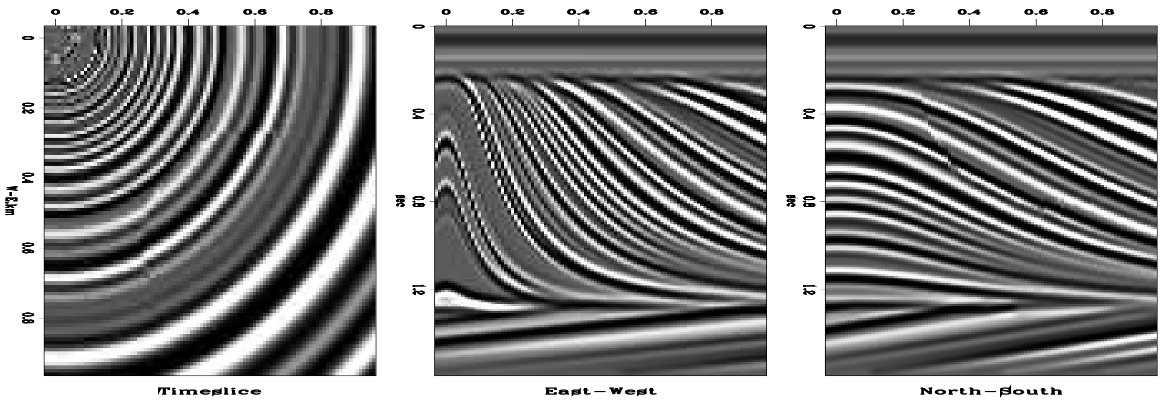

Figure 3: Synthetic image of a delta with a slump fault. From left to right: time-slice from the center of the volume, North-South section from the edge of the volume, East-West section from the center of the volume. The sampling is equal in both spatial directions. The North-South section runs parallel to the delta's gradient and therefore seem to be more steeply dipping than in the center East-West section. The fault is visible in the time-slice and the East-West section. matt2-qdmRaw [CR]

and East-West to refer to the map-view as represented by the time-slice.) The cut is taken at the western edge of the model. Consequently, the section follows the gradient of the bedding and displays the maximal reflector dip of the model. The right image displays a vertical East-West slice that cuts the model at its center. The section intersects the slump fault The section's apparent bedding dip is smaller than the dip in the North-South section, since the center section is not parallel to the bedding's gradient.

Figure 4 displays the Lomoplan output corresponding to the time-slice in Figure 3. The top left plot shows the magnitude of the three Lomoplan output cubes. The other three plots are the individual Lomoplan residuals. Each panel is computed by 2-D prediction error filters operating in a different plane. The top right plot is generated by 2-D planar PE filters that operate in the time-slice plane, as the `TS` of the plot title indicates. The list `a1=1, a2=7, a3=2` of the title expresses the filters' size: no extension in the depth dimension (thus a time-slice filter), seven samples in the North-South dimension, and two samples in the East-West dimension. The bottom right panel corresponds to vertical PE filters predicting in the East-West plane. Finally, the bottom left panel is the output of vertical 2-D PE filters in the North-South plane.

All three Lomoplan residuals in Figure 4 enhance the slump fault. The slump fault is characterized by relatively strong but random output values. All three panels display characteristic noise: the time-slice prediction could not predict the steeply dipping and strongly curving events close to the image's diagonal. At these locations, the synthetic model probably violates our assumption that the model can be locally represented as planar reflector model. The time-slice filter succeeded, however, in removing the same events where they were oriented parallel to one of the filter's axes,

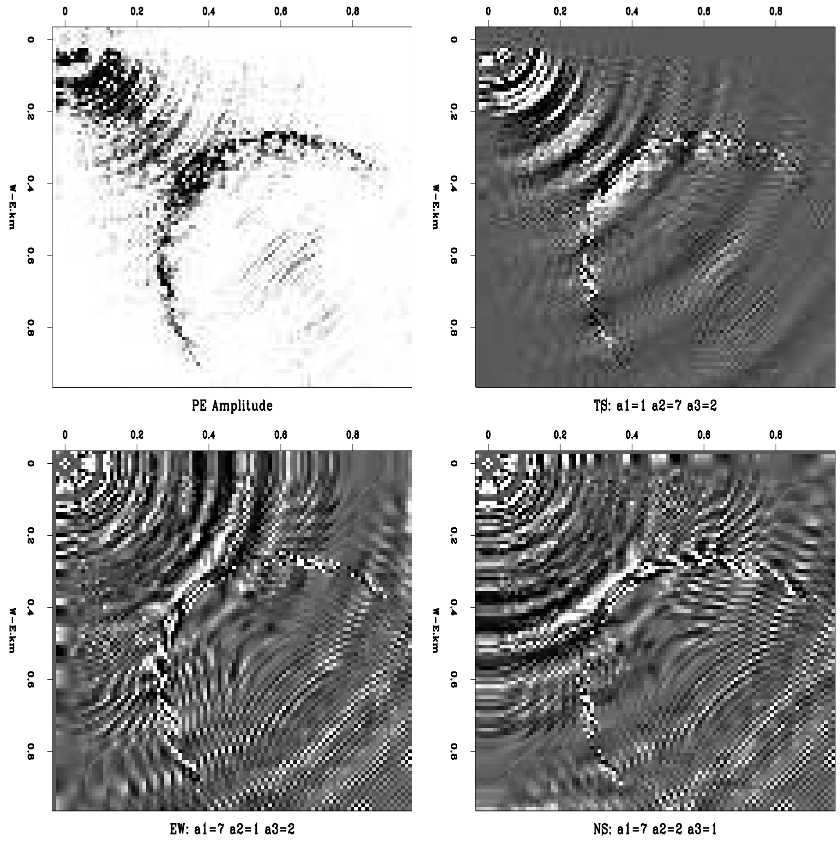

Figure 4: Lomoplan residuals. The figures clockwise from the top-left: Magnitude of the three Lomoplan components and the three Lomoplan outputs (time-slice, East-West, North-South). The time-slice residual has a larger magnitude than the other sections and consequently dominates the magnitude plot. matt2-qdmPef [CR]

as at the northern and western edge of the image. This may indicate unfavorable directional bias that probably results from our filter shape. Both vertical filters display a ringing noise, which might be related to the interpolation that generated the synthetic image. The East-West filter perfectly rejects the East-West striking events at the western edge of the model, but it fails to reject the steeply North-South dipping events at the northern edge of the image. Contrarily, the North-South filter rejects the events at the northern edge, but fails at the western edge. This indicates that the filter with depth stepout of seven coefficients has not sufficed to remove the events of steep apparent dip.

We combined the three Lomoplan outputs by computing the L-2 norm amplitude of the three component vector residual (time-slice, East-West, North-South) at each location. The resulting amplitude at the left top corner of Figure 4 shows no image improvement over the individual residual plots. The time-slice residual dominates the amplitude plot, since its values are an order of magnitude larger than the values of the two vertical residuals. Since the amplitude plot adds positive numbers, the noise is not cancelled. This synthetic model demonstrates our need for a better method to combine the various residual images of Lomoplan.

FIELD DATA EXAMPLES

The figures in this article are clearest on a computer screen. To improve examination of the residual images on paper (which has a lesser dynamic range than a screen), we recolored the white residual with a short triangle filter on the time axis. In the electronic version of this article, the reader can view movies of most image volumes by pressing the figure button.

Fluvial reservoir, Texas

The top-left subsurface time-slice in Figure 5 displays a buried river channel that meanders diagonally from the South-West to the North-East corner. The time-slice possibly contains an entire channel system besides the single visible river channel. The buried river channel is embedded in gently dipping beds that generally strike South-East to North-West and are cut by the channel's sediments. The vertical cross-sections illustrate the gentle reflector dip.

The bottom row of Figure 5 shows a coherency image by CTC[2] The CTC coherency time-slice clearly delineates the edge of the river. In addition to the major river channel, the CTC coherency time-slice displays additional discontinuities which are not obvious in the original image. These events could be spurious events from

[2]We do not want to use the coherency cube for a detailed comparison of the image quality, but prefer to analyze the overall characteristics of the various image volumes. We are responsible for the perhaps less than optimal display of the CTC data by SEP software. CTC mentioned that they could considerably improve the coherency data.

other time-slices or could indicate an underlying channel system that is not visible in the original time-slice. Overall, the image has an almost binary character in which locations are flagged as being part of an edge or of an homogeneous reflector volume.

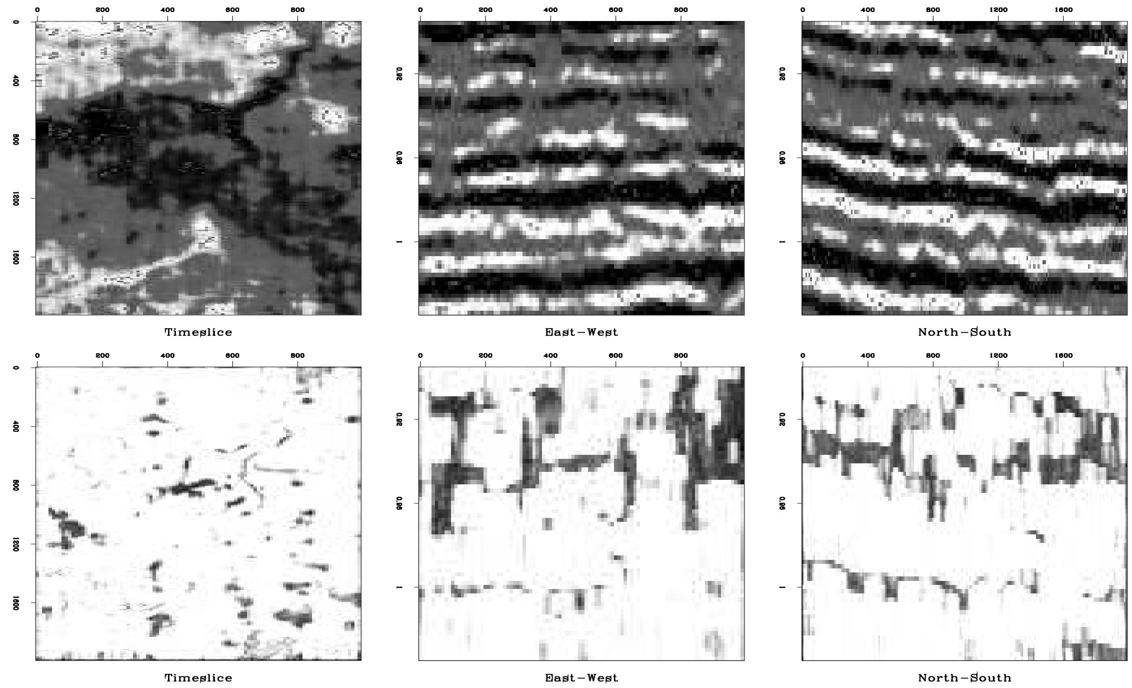

Figure 5: Migrated image and coherency volume of a fluvial reservoir system. The top row displays slices of the migrated image volume, the bottom row displays corresponding slices of a CTC coherency volume. From left to right: time-slice, East-West, and North-South section. matt2-texRaw [CR]

The Lomoplan outputs at the bottom of Figure 6 successfully reject the image's smooth reflectors and delineate the major channel. Unlike the CTC coherency time-slice, the Lomoplan image does not indicate the channel's edge points uniformly. The edges are highlighted by an elusive light-shadow effect that corresponds to the filter's prediction directions. Some isolated strong values in the original data result in some strong-amplitude, high-frequency residuals. Unfortunately, the application of a spatial low-pass filter to the Lomoplan output failed to suppress these events without deteriorating the image of the channel significantly.

Lomoplan does not show the complex channel system that the coherency data shows. This might demonstrate Lomoplan's superior resolution or its inferior sensitivity depending on whether one believes in the existence of the channel system or not.

To highlight the differences between the Lomoplan images and the CTC coherency image, we computed the amplitude spectrum of the various time-slices. Figure 7 displays the original time-slice images in the top row and the corresponding amplitude spectra in the bottom row. Each spectrum is normalized to a total energy of 1 and all spectra are clipped with the same value.

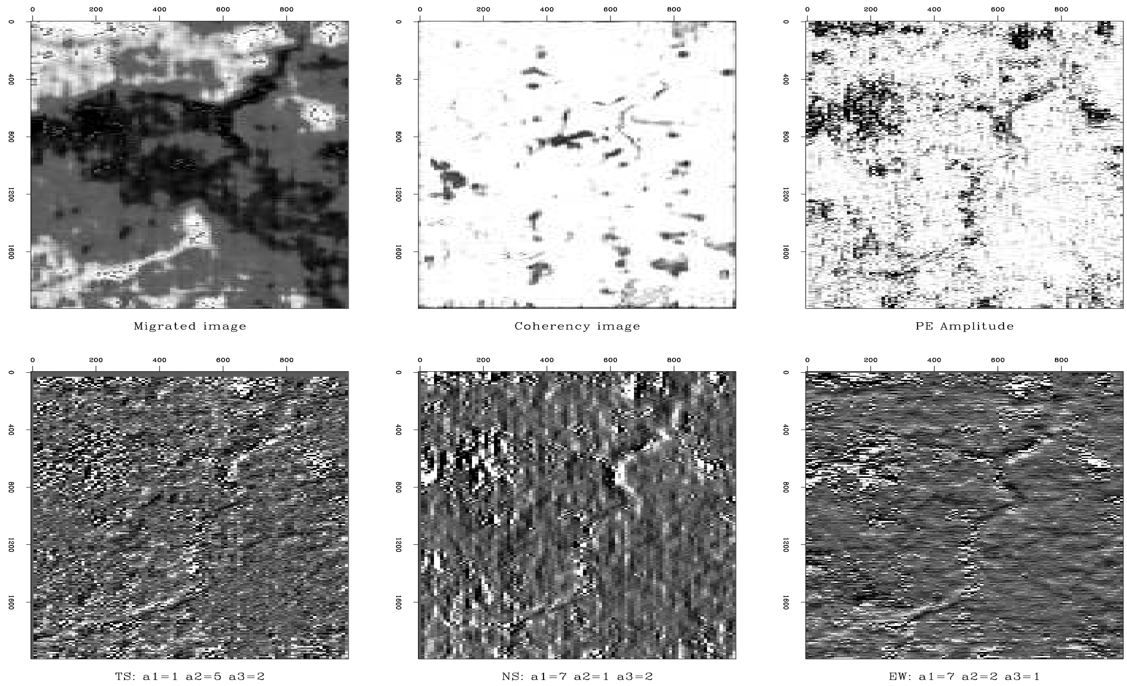

Figure 6: Time-slices of the migrated, Lomoplan and Coherency volumes. Top row: Migrated image, coherency measure, magnitude of the Lomoplan components. Bottom row: Lomoplan outputs with time-slice, East-West, North-South predictions. matt2-texPef [CR]

The original time-slice image has a low frequency power spectrum (see Figure 7). The Lomoplan East-West prediction error filter removes the predictable East-West energy and causes a vertical low energy band in the spectral plot (see bottom center plot of Figure 7). The splitting and merging of the original image to process individual subcubes is not noticeable in the power spectrum. Finally, the power spectrum of the CTC coherency time-slice displays two distinct components: it contains a low frequency component which is similar to the amplitude spectrum of the original subsurface image. Additionally, the spectrum contains a modulated, cross-shaped component along the zero frequency axes. The low frequency component surprised us, since we expected the coherency cube to whiten the spectrum.

Salt dome (Gulf of Mexico)

Figure 8 displays a depth migration image of a salt dome. The time slice cuts the almost circular salt dome in the northeastern corner of the figure. Some hardly visible faults radiate from that salt boundary. The image shows a major, wedge-shaped fault system in the southern half of the time-slice. The North-South striking streaks in the time-slice image are an acquisition footprint, a data artifact caused by the field data's recording geometry and binning. In general, the vertical East-West and North-South sections appear to be noisy and discontinuous (middle and right plot

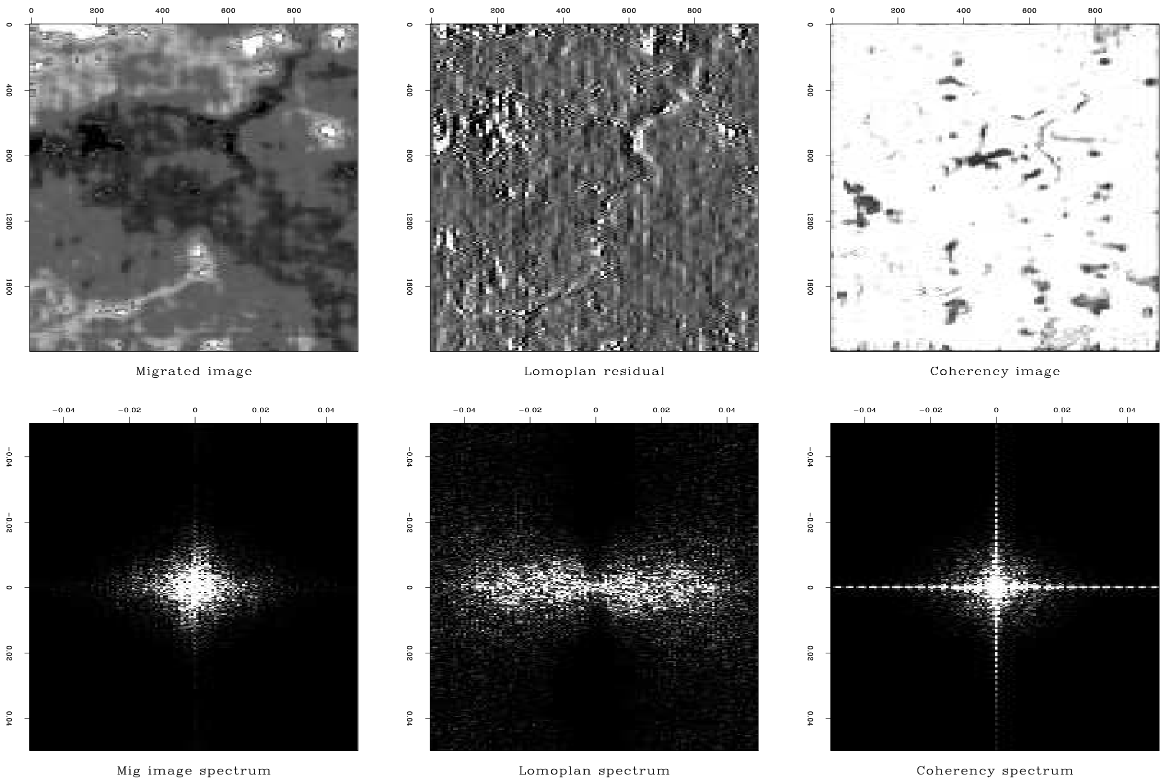

Figure 7: Amplitude spectrum of various time-slice images of a Texan fluvial reservoir system. The top row displays the subsurface images, the bottom row displays the corresponding amplitude spectra (zero frequency is at the center). From left to right: migrated field data, East-West Lomoplan output, CTC image. matt2-texSpc [CR]

of Figure 8). Nevertheless, we discern some steep dipping faults. For example, the reflector depression in the center of the East-West section is bound by the time-slice's southern, wedge-shaped fault system.

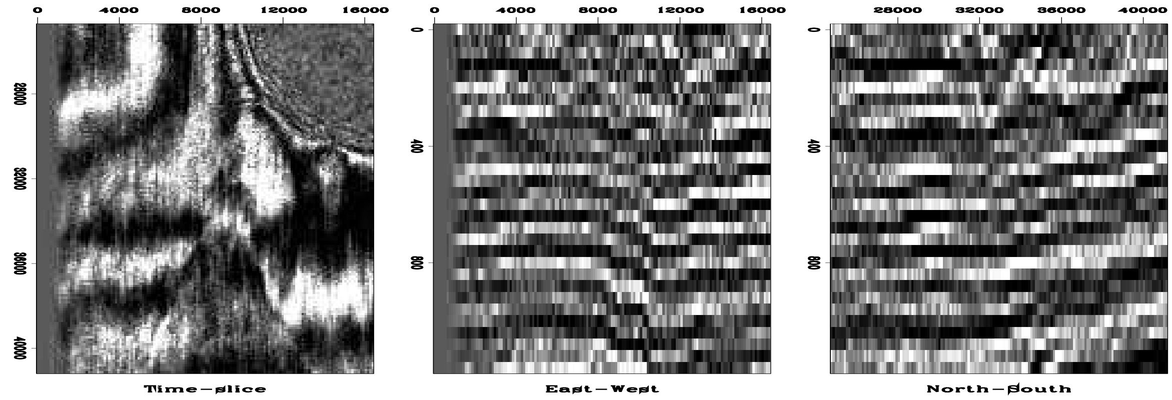

Figure 8: Salt dome in the Gulf of Mexico. The objective is to enhance the faults in the migrated image. From left to right: Time-slice, East-West, and North-South sections. matt2-uniRaw [CR]

As Figure 9 documents, Lomoplan mostly fails to enhance the faults of the salt dome image. The PE filter in the time-slice plane turns the image largely into white noise (top right plot of Figure 9): all events are predictable and therefore removed, except a few minor faults at the salt boundary. The residuals of predicting the low amplitude, incoherent events inside the salt dome are of the same magnitude as the residuals of predicting the high amplitude, but predictable, layered reflectors.

The PE filter in the East-West direction (lower left corner of Figure 9) detects and enhances the acquisition footprint. This North-South striking artifact is unpredictable in the East-West direction and therefore results in large filter residuals. The same North-South streaks are very predictable for filters that predict in the North-South direction, such as the time-slice or North-South residual at the left of Figure 9. Lomoplan could potentially be developed into a method of detecting, estimating, and removing the acquisition footprint of a seismic image after its migration.

The vertical filters (bottom plots of Figure 9) detect the edge of the salt dome. In contrast to the time-slice predictions, the residuals that spring from the salt events are much smaller than the residuals that spring from the surrounding layered reflectors. Unfortunately, we cannot detect the major wedge-shaped fault system in the Lomoplan outputs. These faults were predicted by the various PE filters and were consequently removed. An alternative explanation postulates that the filtered image contains the expected fault residuals, but that other unpredictable events, such as the streaks due to the acquisition footprint or discontinuities between time-slices, overwhelm the fault residuals.

Figure 10 shows the result of applying a single 3-D volume PE filter, rather than the combinations of planar filters, to the salt dome image. The filter does not exclusively reject a local plane reflector component As a matter of fact, in the salt dome

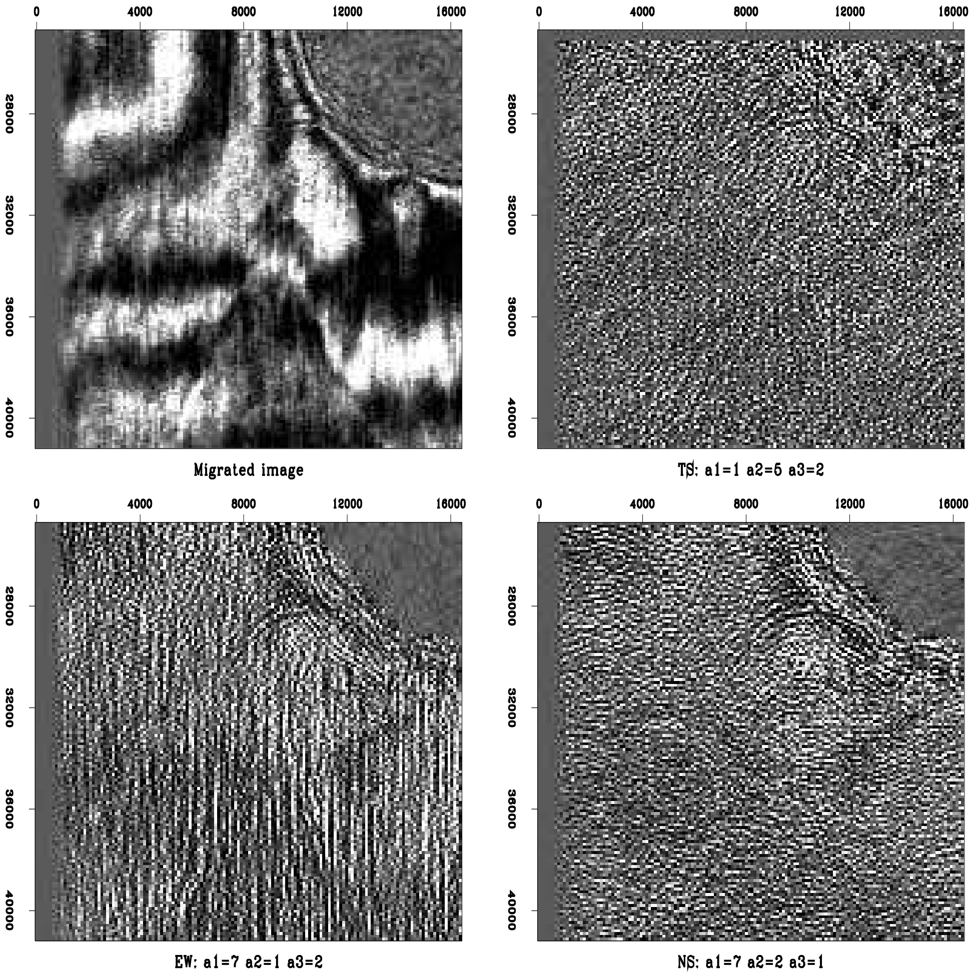

Figure 9: Salt dome in the Gulf of Mexico. Counterclockwise from the top-left: Time-slice of the migrated image, Lomoplan outputs with time-slice, East-West, North-South predictions. matt2-uniPef [CR]

example, even our modestly sized filters manage to predict and remove all events of interest; only the edge of the salt dome remains a distinctive boundary.

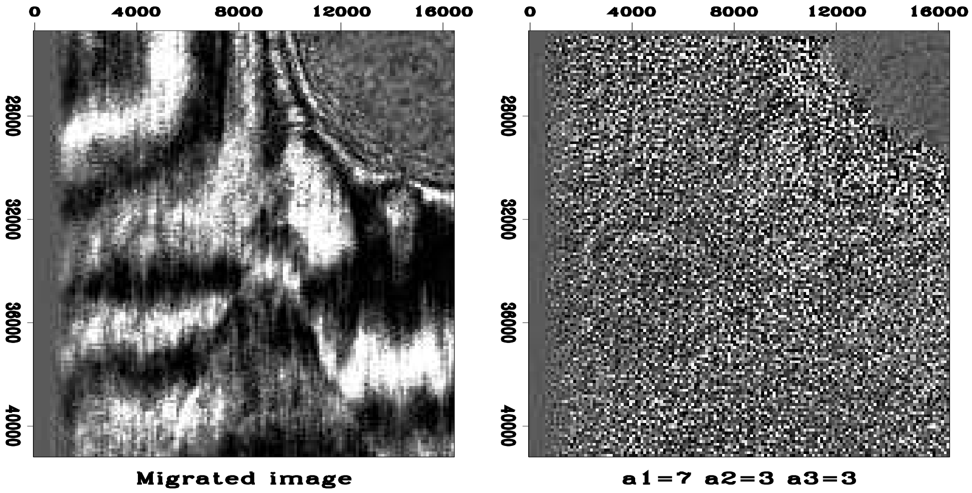

Figure 10: Filtering the migrated image (left) with a single 3-D Prediction Error Filter removes almost all features of interest (right) rather than enhancing them. matt2-uniCub [CR]

Salt anticline (Gulf of Mexico)

Figure 11 images the top of a steep salt anticline. A major normal fault intersects the anticline from southwest to northeast and places the younger rock of the northwestern tip of the anticline next to older sediments of the southeastern anticline part. We want to enhance this major fault in the migrated image and possibly discover additional discontinuities.

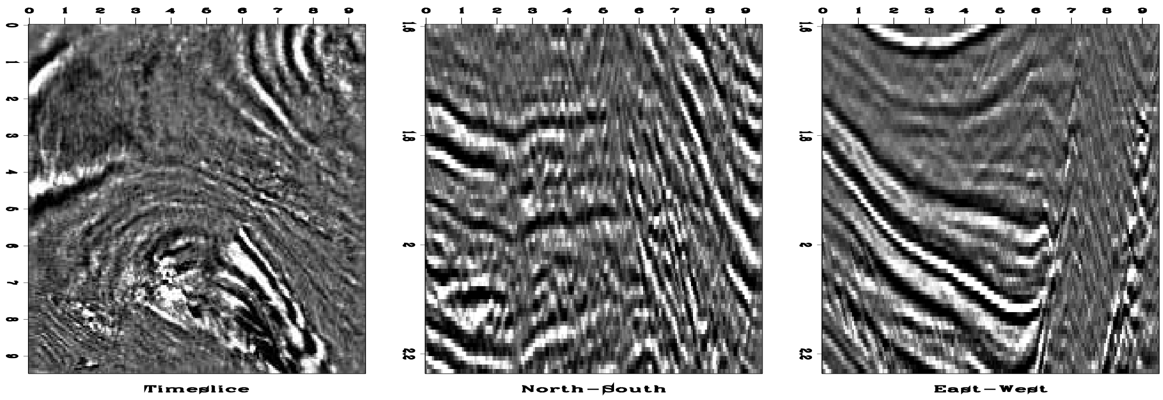

Figure 11: Salt anticline in the Gulf of Mexico. From left to right: time-slice section, vertical East-West section, and North-South section. matt2-halRaw [CR]

As Figure 12 illustrates, Lomoplan removes the smoothly varying part of the wave field but it does not succeed in enhancing the major fault. It also fails to remove the steeply dipping beds in the South-East corner and the strongly curved and disturbed area, where the diagonal normal fault intersects the southern flank of the anticline. Furthermore, the time-slice predictions fail to predict the curved events at the tip of the anticline at the center of the plot. Lomoplan fails to generate an easily interpreted subsurface map.

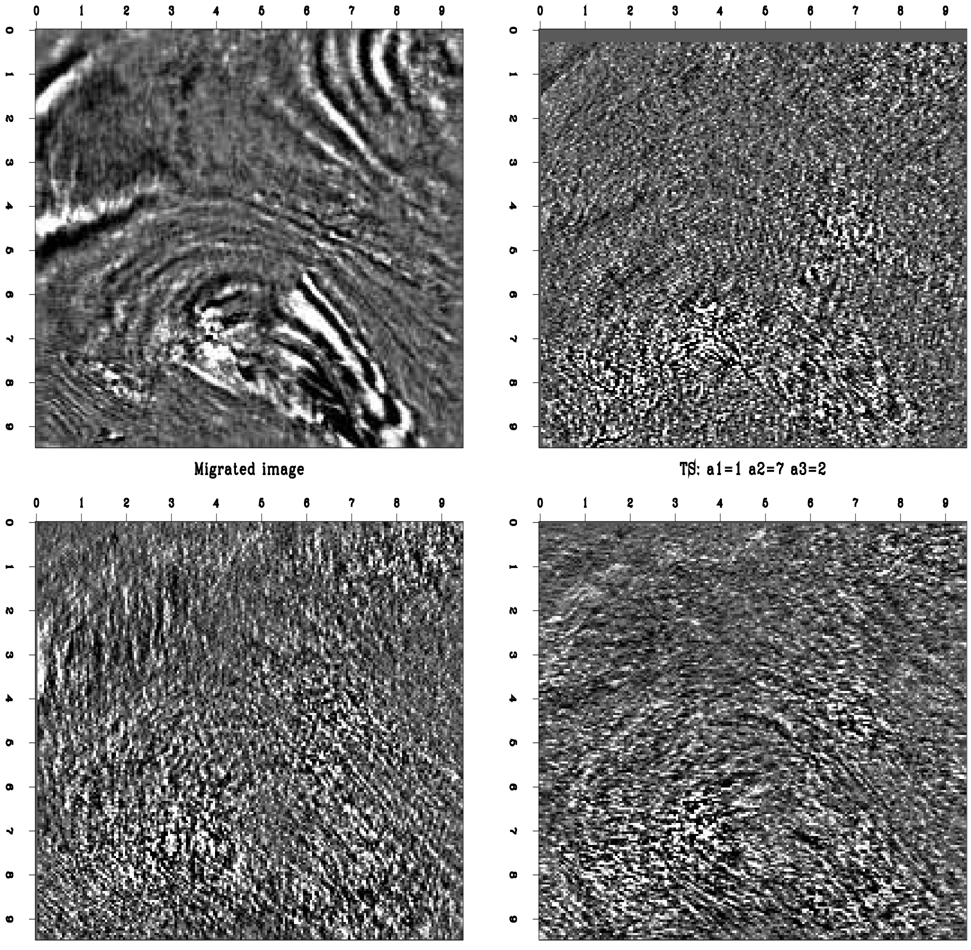

Figure 12: Time-slice of the migrated image (left) and the corresponding Lomoplan amplitude plot (right). matt2-halPef [CR]

To understand better why Lomoplan fails to delineate the major fault, we decided to isolate a single subcube at the intersection of the fault and the northern anticline flank (see Figure 13). Since the subcube's dips are almost stationary over a wide range of cube sizes, we use a single PE filter for the entire subcube. The fault (northeastern trend) and the anticline flank (northwestern trend) cross at the center of the plot.

The residual plots do not depict the strong enhancement of the fault that we initially expected. None of the Lomoplan residual images improves the interpretability compared to the original data.

Inspecting the data closely, we found that the fault is not a sudden, unpredictable

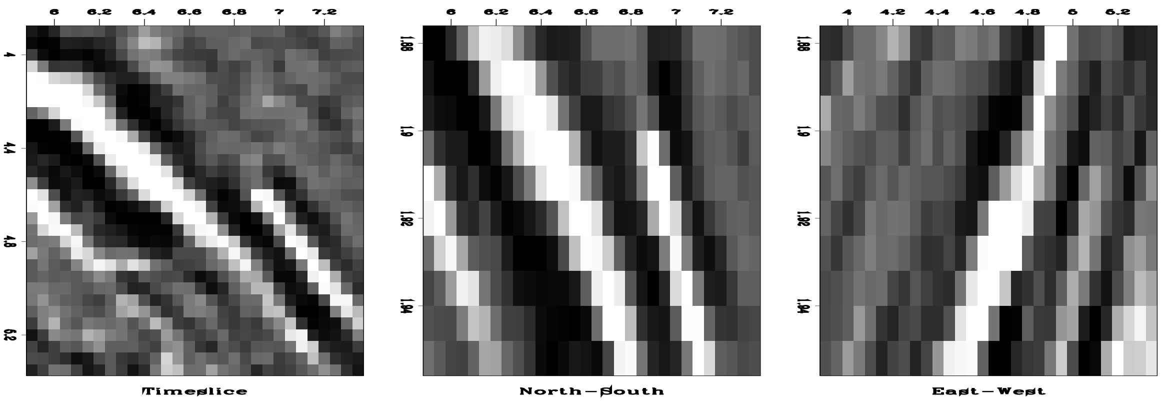

Figure 13: Salt anticline detail. The objective is to enhance the fault striking north-east in the image. From left to right: time-slice section, vertical East-West section, and North-South section. matt2-dhalRaw [ER]

discontinuity, but rather a zone of comparatively rapid amplitude change. However, the fault is several samples wide and rather smooth. Furthermore, the displacement of the sediments is about one wavelength of the sedimentary sequence, which gives a false impression of continuity across the fault zone. For smaller subcubes, the spatial extent of the fault zone and the coincidental continuity of sediments across the fault make it even more difficult for the PE filter to detect the fault location.

The zero valued regions at the edge of Figure 14 result from the particular shape of the PE filters. Since we choose to convolve the filter with known data, the filter's output is smaller than its input, as Figure 15 illustrates. These zero edges are not visible in the final, merged image (such as Figure 12), since the algorithm that merges the subcubes weights the overlapping volumes and their zero-valued edge regions appropriately.

DISCUSSION

We attempted to find a PE filter that removes the local, plane reflector component of an image, and thereby enhances and exposes any subsurface discontinuities, such as erosional surfaces or faults. Since a general PE filter removes any predictable part of the data and whitens its output's power spectrum, we had to restrict the PE filter so that the filter preserves the subsurface's discontinuities. To restrict the filter, we limited its shape to a set of planar 2-D filters which were two columns wide and which had only about ten free coefficients. We did not use the subcube size to tune which events are predictable and which are not. Instead, we strove for small subcubes that promise an optimal resolution.

Despite our efforts to restrict the PE filter, the filter usually removed most discontinuities that we were seeking to enhance. Our restrictions failed, because our assumptions about the subsurface were partially wrong: geological discontinuities in

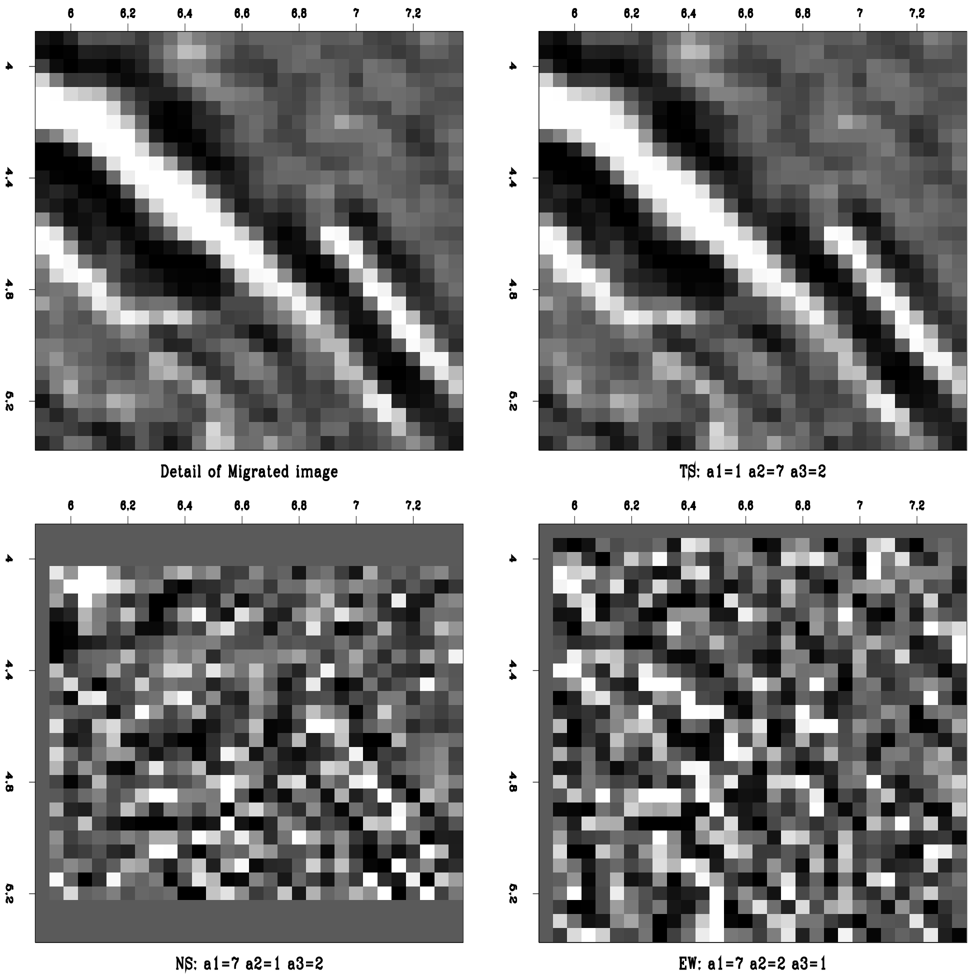

Figure 14: Detail of salt anticline. Counterclockwise from the top-left: Time-slice of the migrated image, Lomoplan outputs with time-slice, East-West, North-South predictions. matt2-dhalPef [ER]

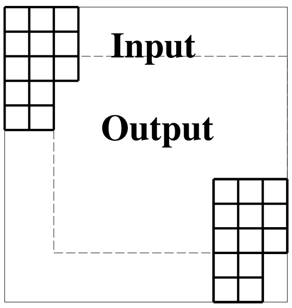

Figure 15: Domain of inputs and outputs of a two-dimensional prediction-error filter. matt2-rabdomain [NR]

a seismic subsurface image are usually zones of rapid but continuous transition (often several pixels wide) and not singular discontinuous boundaries. Consequently, we need to develop ways of tuning the filter process to reject certain bandwidths while preserving others.

The PE filter framework itself offers several potential remedies: we can

- low-pass filter the residuals.
- introduce gaps in the PE filters which limits the filters' ability to predict and consequently remove rapidly varying image features.
- prewhiten the input data, before using the PE filter described in this article.

The PE filter approach was easy to test because we had developed the necessary software. Obviously, there are alternative filter techniques (such as traditional edge detection schemes) that we may want to pursue alternatively.

A working coherency measure could possibly be an important building block in a library of data visualization and processing tools. A natural extension of the image processing aspect of the coherency measure could be software that picks the enhanced surfaces and delivers the interpreter a proposed set of continuous surfaces (e.g., as a GOCAD model). The coherency image could be complemented by other local data attributes, such as instantaneous frequency or seismic amplitude. An ambitious data analysis and visualization software could combine statistics of the image subcube, of the migrated data that stacks to the image subcube, and of the raw data that contributes to the image subcube.

CONCLUSION

The PE filter technique (Lomoplan) that we presented in this article was designed to enhance discontinuities in migrated seismic subsurface images. The PE filter technique, called Lomoplan, proved difficult to tune for the target in a particular data set. After an initial success (Fluvial system), we encountered later cases for which the filter

- enhanced image artifacts in an image (salt dome) that contained a strong acquisition footprint.
- removed all the discontinuities in an image (salt anticline) whose discontinuities were smooth.

Additionally, we lack a meaningful method of combining the output of the various Lomoplan residual images. Overall, we have yet failed to devise a robust process that enhances discontinuities.

ACKNOWLEDGMENTS

Ray Abma contributed several drawn figures which illustrate the underlying filter technique. David Lumley made his migrated image of the salt anticline data available. Mihai Popovici obtained the image of the Texan fluvial reservoir and the corresponding coherency cube from CTC.

Sudhakar Vasudhaven of CTC made the Texan fluvial reservoir images available. Wook Lee of Unocal provided the salt dome data to SEP. Haliburton Geophysical Services released the salt anticline data to SEP. Without their help, this work would have been a tedious theoretical paper with an incorrect conclusion.

REFERENCES

Claerbout, J. F., 1976, Fundamentals of geophysical data processing: Blackwell.

Claerbout, J. F., 1992, Information from smiles: Mono-plane-annihilator weighted regression: SEP–**73**, 409–420.

Claerbout, J. F., 1993, 3-D local-monoplane annihilator: SEP–**77**, 19–26.

Claerbout, J. F., 1994, Applications of Three-Dimensional Filtering: Stanford Exploration Project.

Haskell, N. L., Nissen, S. E., Lopez, J. A., and Bahorich, M. S., 1995, 3-D seismic coherency and the imaging of sedimentological features: 65th Ann. Internat. Mtg., Soc. Expl. Geophys., Expanded Abstracts, 1532–1534.

Marfurt, K. J., Scheet, R. M., Sharp, J. A., Cain, G. J., and Harper, M. G., 1995, Suppression of the acquisition footprint for seismic sequence attribute mapping: 65th Ann. Internat. Mtg., Soc. Expl. Geophys., Expanded Abstracts, 949–952.

Nissen, S. E., Haskell, N. L., Lopez, J. A., Donlon, T. J., and Bahorich, M. S., 1995, 3-D seismic coherency techniques applied to the identification and delineation of slump features: 65th Ann. Internat. Mtg., Soc. Expl. Geophys., Expanded Abstracts, 1535–1536.

APPENDIX A

We want to prove that for a given $\mathbf{p} = (p_x, p_y, p_z)$ the expression

$$(p_y\partial_z - p_z\partial_y,\ -p_x\partial_z + p_z\partial_x,\ p_x\partial_y - p_y\partial_x)\ \tilde{g}(x,y,z) \tag{A-1}$$

vanishes for all $\mathbf{x} = (x, y, z)$, if and only if $\tilde{g}$ is a volume of parallel planes, $\tilde{g} = g(p_x x + p_y y + p_z z)$. ($\mathbf{p}$ represents the strike of the parallel planes; g represents a one-dimensional amplitude function).

First, we prove that expression (A-1) vanishes for a volume of parallel, planes. Applying the chain rule to the first component $(p_y\partial_z - p_z\partial_y)g(p_x x + p_y y + p_z z)$ yields $(p_y g' p_z - p_z g' p_y) = 0$. An analogue result for the two additional components of expression (A-1) demonstrates that the entire expression vanishes for a volume $\tilde{g}$ that consists of parallel planes.

Next, we prove that if all three components of expression (A-1) vanish, than the function $\tilde{g}$ is a volume of parallel planes. We set the expression (A-1) to zero and express it as a vector product of $\mathbf{p}$ and the gradient of the field, ∇g:

$$\mathbf{0} = \begin{pmatrix} p_y\partial_z - p_z\partial_y \\ -p_x\partial_z + p_z\partial_x \\ p_x\partial_y - p_y\partial_x \end{pmatrix} g = (\mathbf{p} \times \nabla g) \tag{A-2}$$

The vector product of $\mathbf{p}$ and ∇g is zero if and only if one of the vectors is the null vector, or if the vectors are parallel. Ignoring the trivial cases, we conclude that when the outputs of the three finite difference filters vanish everywhere, than the gradient of g is parallel to the constant vector $\mathbf{p}$. The constant $\mathbf{p}$ is normal to g at all locations and therefore g has to be a volume of parallel planes.

Geometric interpretation

This proof offers an interpretation of the Lomoplan outputs. When Lomoplan first computes the filter coefficients, it estimates the vector $\mathbf{p}$. The filter coefficients capture the inverse (dip) spectrum of the local subcube. The application of the filter within the subcube computes at every location the vector product of the overall gradient of the subcube and the gradient at that specific location, $\|\mathbf{p}\|\|\nabla g\|\sin(\alpha)\mathbf{n}$. ($\alpha$ is the angle between $\mathbf{p}$ and the gradient ∇g; $\mathbf{n}$ is the normal to the plane spanned by $\mathbf{p}$ and ∇g).

Remarks

We consider expression (A-1) the lowest order finite difference filter that destroys exclusively planes. The expression (A-1) and the proof above can be reformulated so that it includes a normalized vector $\mathbf{p}$ and only two instead of three components.

A zero output of neither a single component equation (A-1) nor a single 3-D filter suffice to conclude that the function g is a volume of parallel planes. For example, the first component $(p_y\partial_z - p_z\partial_y)$ applied to a volume of parallel lines $h(x, p_y y + p_z z)$ would yield zero, but h is not a volume of parallel planes. In contrast, a 3-D volume filter removes events other than parallel planes. Similarly, a 3-D filter removes the volume of parallel lines $h(x, p_y y + p_z z)$.

Nevertheless, our filter formulation might be more restrictive than necessary: essentially, we do not care how the filter operates on events that it does not encounter in seismic subsurface images.